Molecular Therapy
Nucleic Acids
Original Article

Spherical Nucleic Acid Architecture Can Improve the Efficacy of Polycation-Mediated siRNA Delivery

Jilian R. Melamed,[1] Nicole L. Kreuzberger,[1] Ritu Goyal,[1] and Emily S. Day[1,2,3]

[1]Biomedical Engineering, University of Delaware, Newark, DE 19716, USA; [2]Materials Science & Engineering, University of Delaware, Newark, DE 19716, USA; [3]Helen F. Graham Cancer Center and Research Institute, Newark, DE 19713, USA

Clinical translation of small interfering RNA (siRNA) nanocarriers is hindered by limited knowledge regarding the parameters that regulate interactions between nanocarriers and biological systems. To address this, we investigated the influence of polycation-based nanocarrier architecture on intracellular siRNA delivery. We compared the cellular interactions of two polycation-based siRNA carriers that have similar size and surface charge but different siRNA orientation: (1) polyethylenimine-coated spherical nucleic acids (PEI-SNAs), in which polyethylenimine is wrapped around a spherical nucleic acid core containing radially oriented siRNA and (2) randomly assembled polyethylenimine-siRNA polyplexes that lack controlled architecture. We found that PEI-SNAs undergo enhanced and more rapid cellular uptake than polyplexes, suggesting a prominent role for architecture in cellular uptake. Confocal microscopy studies demonstrated that while PEI-SNAs and polyplexes exhibit similar intracellular stability, PEI-SNAs undergo decreased accumulation within lysosomes, identifying another advantage conferred by their architecture. Indeed, these advantageous cellular interactions enhanced the gene silencing potency of PEI-SNAs by 10-fold relative to polyplexes. Finally, cytocompatibility studies showed that PEI-SNAs exhibit decreased toxicity per PEI content relative to polyplexes, allowing the use of more polycation. Our studies provide critical insight into design considerations for engineering siRNA carriers and warrant future investigation of how nanocarrier architecture influences cellular-, organ-, and organism-level interactions.

INTRODUCTION

Despite the exciting therapeutic potential of small interfering RNA (siRNA)-mediated gene silencing to treat diseases with a genetic basis, physiological barriers to siRNA delivery have hindered its clinical translation. siRNA is highly susceptible to nuclease degradation, is rapidly cleared from circulation, and cannot passively enter cells due to its large size and negative charge. Consequently, novel carriers are needed to enable the clinical translation of siRNA. To successfully deliver siRNA, intravenously injected carriers must evade immune clearance from the bloodstream, transport across the vascular endothelium to reach the target tissue, diffuse through the extracellular matrix, enter the diseased cells, escape from endocytic vesicles, and deliver siRNA to the RNA-induced silencing complex (RISC).[1] These unresolved challenges have prompted widespread investigation of nanoscale materials to effectively protect and deliver siRNA to diseased tissues.

Polycationic nanoscale materials have demonstrated broad utility for nucleic acid delivery due to their abilities to condense and protect nucleic acids from nucleases and rapidly enter cells.[2,3] Such materials include synthetic polymers and polymers derived from amino acids, cell penetrating peptides inspired by viruses, and lipid-based carriers. As a potent polycation containing a high density of amine groups, polyethylenimine (PEI) is among the most widely investigated synthetic polymers for nucleic acid delivery.[4,5] This is in large part because PEI can enable nucleic acid escape from intracellular endocytic vesicles due to its high buffering capacity,[6,7] overcoming a significant cellular barrier to nucleic acid delivery. Further, PEI is attractive from an engineering standpoint for its wide availability in a range of molecular weights and degrees of branching, low cost, and ease of modification for multimodal delivery systems.[5]

However, PEI and other polycationic materials are plagued by toxicity that precludes their clinical utility. This high toxicity is due to the presence of primary amines that impart a high positive charge. Indeed, PEI destabilizes cellular membranes, induces mitochondrial dysfunction, and may trigger complement activation *in vivo*.[4] Consequently, numerous efforts are ongoing to modify PEI to mitigate its cytotoxic effects while retaining its potent nucleic acid delivery efficacy.[4,5,8] Toward this goal, we hypothesized that changing the architecture and presentation of PEI to target cells may enhance siRNA delivery while minimizing cytotoxicity. Here, we demonstrate that hybrid polycationic-nanoparticle carriers can outperform standalone polycations, supporting the growing body of literature that suggests nanoscale architecture and surface chemistry play key roles in gene silencing.

Received 18 April 2018; accepted 10 May 2018;
https://doi.org/10.1016/j.omtn.2018.05.008.

Correspondence: Emily S. Day, University of Delaware, 161 Colburn Lab, Newark, DE 19716, USA.
E-mail: emilyday@udel.edu

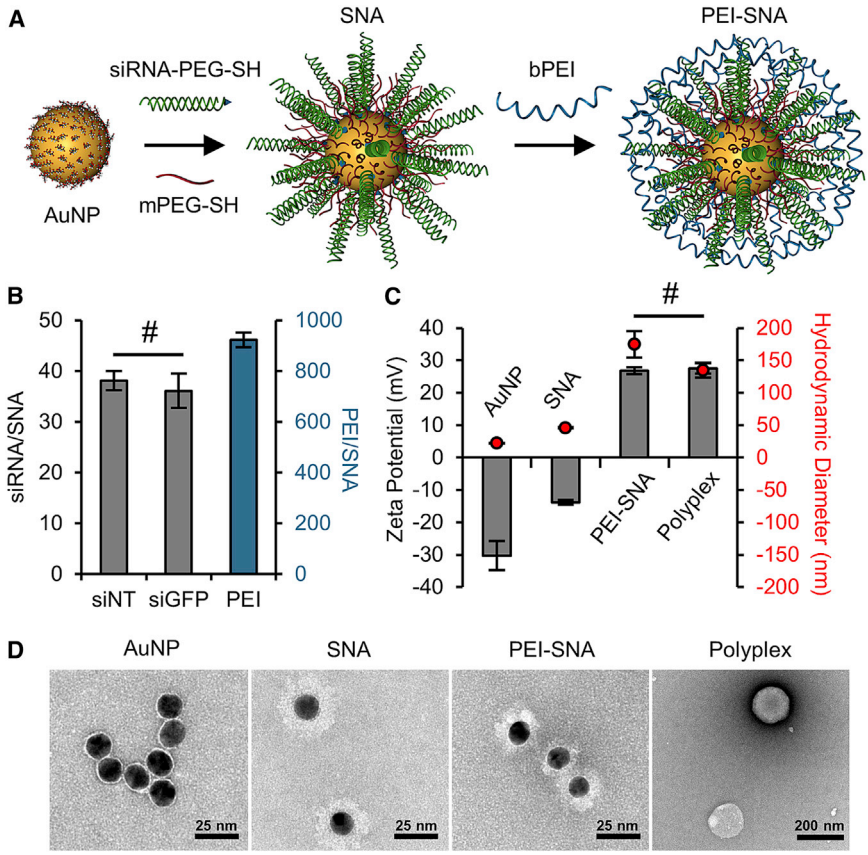

Figure 1. Nanoparticle and Polyplex Synthesis and Characterization

(A) Schematic describing the synthesis of SNAs and PEI-SNAs. (B) siRNA and PEI loading characterization on SNAs and PEI-SNAs. Data are means ± SDs; #, no significance. (C) Zeta potential and DLS measurements for AuNPs, SNAs, PEI-SNAs, and PEI-siRNA polyplexes. Data are means ± SDs; #, no significance. (D) Representative TEM images of AuNPs, SNAs, PEI-SNAs, and polyplexes. Grids were counterstained with uranyl acetate to visualize siRNA as light contrast.

In this study, we exploit the unique surface structure of spherical nucleic acid nanoparticles (SNAs) as agents to modify PEI presentation to cells in a hybrid delivery system. SNAs have recently emerged as a new class of gene regulatory agents with attractive properties that may potentiate the gene silencing capacity of PEI-based siRNA carriers. SNAs consist of a spherical nanoparticle core coated with densely packed nucleic acids that are oriented radially from the core surface.[9,10] This architecture imparts distinct properties that favor nucleic acid delivery in biological systems. Most notably, SNAs undergo cellular entry without the need for ancillary transfection agents, exhibit enhanced stability against nucleases due to steric and electrostatic hindrances provided by their architecture, and demonstrate excellent biocompatibility in animal models.[11–13] Further, this architecture has been previously demonstrated to facilitate siRNA complexation with poly(β-amino ester)s, which fail to form complete nanoparticles with unbound siRNA likely due to the rigidity of siRNA molecules.[14] SNAs have been previously demonstrated to effectively deliver siRNA and microRNA to glioblastoma tumors following systemic injection,[15,16] and their success in animal models has recently prompted the first clinical trial investigating these constructs as therapeutics for glioblastoma multiforme and gliosarcoma.[17]

To test our overarching hypothesis that nanoscale architecture can improve polycation-mediated siRNA delivery, we investigate the cellular uptake, intracellular trafficking, cytocompatibility, and gene regulation efficacy of PEI-coated SNAs (PEI-SNAs) versus PEI-siRNA polyplexes. We find that PEI-SNAs undergo enhanced cellular uptake relative to both SNAs and polyplexes and exhibit reduced accumulation within lysosomes relative to polyplexes. The improved uptake and trafficking profile achieved with PEI-SNAs translates to dramatically enhanced gene silencing capabilities using lower siRNA doses. Importantly, potent gene silencing with PEI-SNAs is achieved within a cytocompatible dosing range. Taken together, our data demonstrate the potential for the unique architecture of SNAs to improve the gene regulation efficiency of polycationic materials and vice versa, for cationic materials to improve the gene regulation efficiency of SNAs. These observations confirm that nanoscale architecture and surface chemistry play a critical role in gene regulation and warrant further investigation of the intracellular trafficking mechanisms responsible for determining the fate of hybrid cationic-nanoparticle siRNA carriers.

RESULTS

Nanoparticle and Polyplex Synthesis and Characterization

Citrate-capped 15 nm gold nanoparticles (AuNPs) were prepared in-house using the Frens method[18] and subsequently functionalized with siRNA and polyethylene glycol (PEG) via thiolated ligands according to established procedures to produce SNAs.[15,19] To prepare PEI-SNAs, purified SNAs were coated with PEI via electrostatic adsorption, and purified again to remove unbound PEI (Figure 1A). An OliGreen assay[19] revealed that SNAs contained ~38 siRNA duplexes per particle, and a 2,4,6-trinitrobenzene sulfonic acid (TNBS) assay[20] determined that ~923 PEI molecules are associated with each PEI-SNA (Figure 1B). At each step, the resulting AuNP conjugates were characterized using UV-visible spectroscopy, dynamic light scattering (DLS), zeta potential, and transmission electron microscopy (TEM). PEI-siRNA polyplexes were produced using standard methods with an N/P ratio of 6 (Figure S1).[21] This N/P ratio was chosen to completely complex siRNA with PEI, as demonstrated by a gel retardation assay (Figure S1B) and to optimally balance transfection

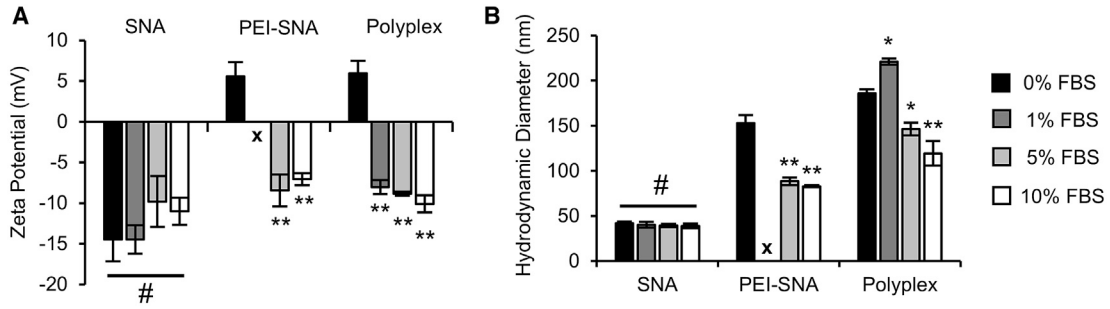

Figure 2. Serum Stability of SNAs, PEI-SNAs, and Polyplexes

(A) Zeta potential and (B) DLS measurements for SNAs, PEI-SNAs, and polyplexes incubated in FBS. Data are means ± SDs. X, could not record accurate measurement due to severe aggregation; #, no significant difference; *p < 0.01 relative to 0% FBS control; **p < 0.0001.

efficiency promoted by higher N/P polyplexes[22] with cytotoxicity (Figure S1C). Polyplexes were further characterized by DLS, TEM, and zeta potential measurements.

Functionalizing AuNPs with siRNA and PEG increased the hydrodynamic diameter from 22 nm to 46 nm, and coating with PEI further increased the hydrodynamic diameter to ~175 nm, similar in size to the ~140 nm polyplexes (Figure 1C). Because UV-visible spectroscopy (Figure S2) did not reveal any signs of aggregation (i.e., broadening or red shifting of the characteristic ~520 nm AuNP absorbance maximum) and monodisperse PEI-SNAs were visible by TEM (Figure 1D), we attributed this large increase to the size and number of PEI molecules associated with each PEI-SNA rather than to particle aggregation. Zeta potential measurements further confirmed successful functionalization, with AuNPs and SNAs exhibiting net negative surface charges (−30 mV and −14 mV, respectively), while PEI-SNAs and polyplexes exhibited net positive surface charges (both ~27 mV) (Figure 1C).

Evaluation of PEI-SNA and Polyplex Serum Stability

To assess the serum stability of PEI-SNAs and polyplexes, constructs were incubated in 1%, 5%, or 10% fetal bovine serum (FBS) for 2 hr and subsequently evaluated by zeta potential measurements and DLS to determine whether or not exposure to serum affects their surface chemistry or colloidal stability. PEI-SNAs suspended in 1% FBS aggregated quickly and visibly crashed out of solution, while PEI-SNAs remained stabled in 5%–10% FBS. This indicates that serum proteins are crucial for maintaining the colloidal stability of PEI-SNAs. Following two hours incubation with FBS, both PEI-SNAs and polyplexes undergo charge reversal and maintain zeta potential values of approximately −8 mV for all tested FBS concentrations (Figure 2A), indicating that negatively charged serum proteins associate with both particle types. For comparison, SNAs do not undergo significant changes in zeta potential under the same conditions. We further investigated the effects of serum on hydrodynamic diameter (Figure 2B). Surprisingly, both PEI-SNAs and polyplexes exhibited significant decreases in hydrodynamic diameter after incubation with 5%–10% FBS. Taken together, these results lead us to speculate that serum proteins displace PEI that is loosely bound to the periphery of both particle types and that this interaction induces a stabilizing effect.

PEI-SNAs Undergo Enhanced Cellular Binding and Uptake Than PEI-siRNA Polyplexes or SNAs

Flow cytometry was used to quantitatively examine the extent to which and rate at which U87-MG glioma cells bind and internalize SNAs, PEI-SNAs, or polyplexes prepared with Cy5-labeled siRNA. SNAs exhibited the lowest degree of binding and uptake after 24 hr and achieved maximum cellular siRNA fluorescence intensity after 4 hr of continuous incubation with U87-MG cells (Figures 3A and 3B). In contrast, polyplexes and PEI-SNAs undergo increasing binding and uptake through 24 hr of continuous incubation with U87-MG cells and achieve 5- or 81-fold increases in cellular siRNA fluorescence intensity relative to SNAs, respectively (Figures 3A and 3B), after 24 hr. Further, binding and uptake of PEI-SNAs occurs far more rapidly than that of polyplexes, with cellular accumulation of Cy5-siRNA appearing within 15 min when delivered via PEI-SNAs versus 4 hours via polyplexes. PEI-SNAs achieve a 28-fold increase in cellular Cy5-siRNA intensity relative to polyplexes over 4 hr and a 16.5-fold increase over 24 hr (Figures 3A and 3B). The increased binding and uptake of polyplexes and PEI-SNAs relative to SNAs is likely due to their equivalent net positive surface charge, but we attribute the dramatically enhanced uptake of PEI-SNAs relative to polyplexes to differences in surface structure resulting from the spherical architecture of SNAs.

PEI-SNAs and Polyplexes Remain Intact following Endocytosis

To determine whether siRNA dissociates from either PEI-SNAs or polyplexes following endocytosis, confocal microscopy was used to observe the relative intracellular trafficking of Cy5-siRNA and tetramethylrhodamine isothiocyanate (TRITC)-PEI from each carrier. Cy5-TRITC-PEI-SNAs and Cy5-TRITC-polypexes were characterized using DLS and zeta potential measurements (Figure S3). Cells were incubated with PEI-SNAs or polyplexes for 24 hr, then imaged or incubated a further 24 hr prior to imaging. Quantitative colocalization analysis was employed to calculate the fractional overlap of Cy5-siRNA and TRITC-PEI using Mander's colocalization coefficients (MCC). Our studies demonstrate that siRNA and PEI from

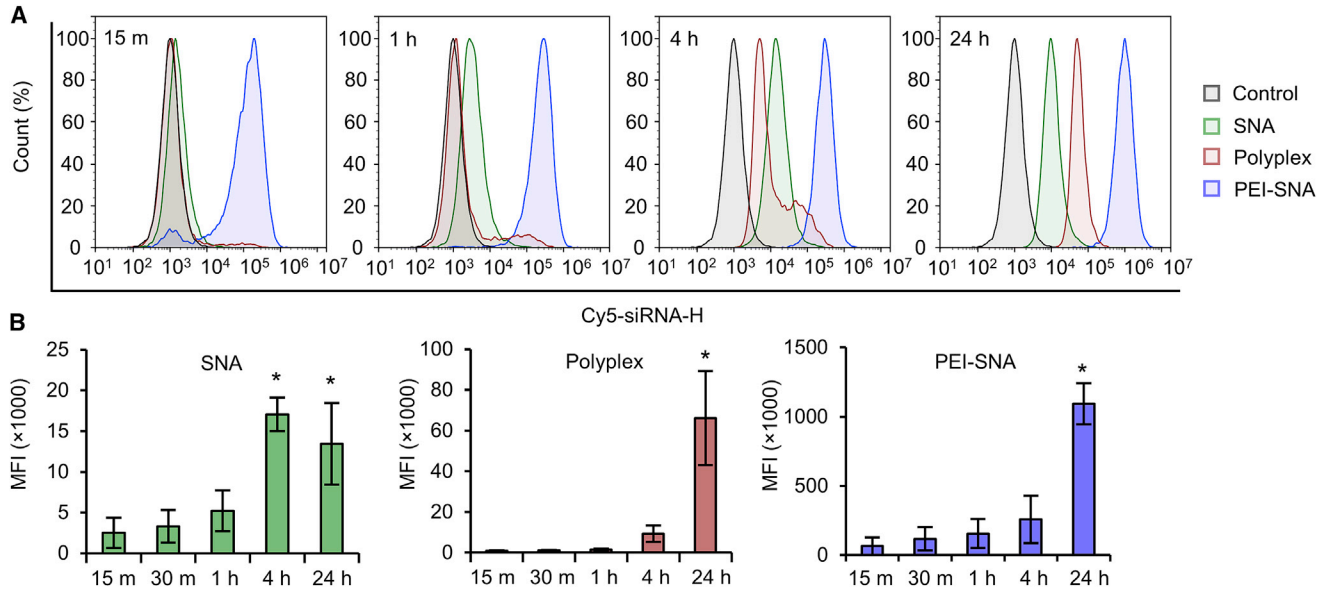

Figure 3. Extent and Kinetics of Nanocarrier Binding/Internalization Depends on Nanocarrier Surface Chemistry and Architecture

(A) Representative flow cytometric histograms showing cellular uptake of equivalent Cy5-siRNA payloads via SNAs, polyplexes, and PEI-SNAs with increasing incubation times. (B) Summary of flow cytometry data in (A) across three independent experiments. Data are median fluorescence intensities (MFI) ± SDs; *p < 0.01.

both carriers remain heavily colocalized (all MCC ~0.95) up to 48 hr after delivery to cells (Figures 4A–4C and S4). These data demonstrate that either complete siRNA dissociation from the carrier is not necessary to enable gene silencing or that the fraction of dissociated siRNA is too small to detect using these methods. However, we are encouraged that PEI-SNAs exhibit stability in physiological conditions at least equal to that of polyplexes, which have been widely investigated through *in vivo* gene regulation studies.[4] Thus, this data supports the use of polycation-wrapped SNAs as potentially translatable siRNA carriers.

PEI-SNAs Exhibit Decreased Lysosomal Accumulation Relative to PEI-siRNA Polyplexes

An unresolved challenge to nanoparticle-mediated siRNA delivery is maximizing the release of internalized cargo from endocytic vesicles into the cytosol to interact with RNAi machinery and achieve gene silencing. This is evident in recent research demonstrating that only ~1%–2% of internalized siRNA reaches the cytosol to regulate gene expression.[23,24] In the classical endocytic pathway, siRNA nanocarriers interact with cellular surface receptors to initiate endocytosis, are taken up into early endosomes, then are trafficked through late endosomes until finally reaching lysosomal compartments, where they are enzymatically degraded. First, we demonstrated that both PEI-SNAs and polyplexes undergo endocytosis by visualizing their uptake into $Rab5^+$ early endosomes. $Rab5^+$ early endosomes were labeled by stably expressing a Rab5-GFP fusion protein in U87-MG cells, and PEI-SNAs or polyplexes were labeled using Cy5-siRNA. Cells were treated with PEI-SNAs or polyplexes and imaged immediately. Using confocal microscopy, we found that PEI-SNAs could be first detected within $Rab5^+$ early endosomes within 60 to 90 min (Figure 5A). Consistent with our previous flow cytometry data, polyplex internalization appeared slightly slower, with early endosomal accumulation detectable within 120 min (Figure 5A). Because successful siRNA nanocarriers should minimize lysosomal accumulation to prevent the degradation of internalized siRNA, we investigated the degree of nanocarrier colocalization with lysosomes using cells stably expressing LAMP1-GFP. Cells were incubated with PEI-SNAs or polyplexes for 24 hr, washed to remove unbound particles, then imaged live using confocal microscopy (Figure 5B). Quantitative colocalization analysis was conducted to calculate the fractional overlap of each probe. Excitingly, PEI-SNAs demonstrated a significant decrease in colocalization with lysosomes relative to polyplexes (Figure 5C; MCC = 0.83 for polyplexes and MCC = 0.75 for PEI-SNAs). For comparison, SNAs lacking a PEI coating exhibited high accumulation within lysosomes, similar to polyplexes (MCC = 0.85; Figure S5). Because endosomal escape is well understood to be a highly inefficient process,[24] we believe the observed 8% decrease in lysosomal accumulation for PEI-SNAs relative to polyplexes is biologically impactful. There was no significant difference in the fractional overlap of LAMP1-GFP with Cy5-siRNA for PEI-SNAs and polyplexes, indicating that the fraction of total lysosomes containing siRNA is the same in each case (Figure 5D).

PEI-SNAs Mediate GFP Silencing at Dramatically Lower siRNA Doses Than PEI-siRNA Polyplexes

To compare the gene silencing potency of polyplexes and PEI-SNAs, we targeted GFP as a model gene in U373 glioblastoma cells stably expressing EGFP. Cells were treated with polyplexes or PEI-SNAs at various siRNA payloads for 24 hr in complete culture medium, replenished with fresh medium, and incubated a further 24 hr, then

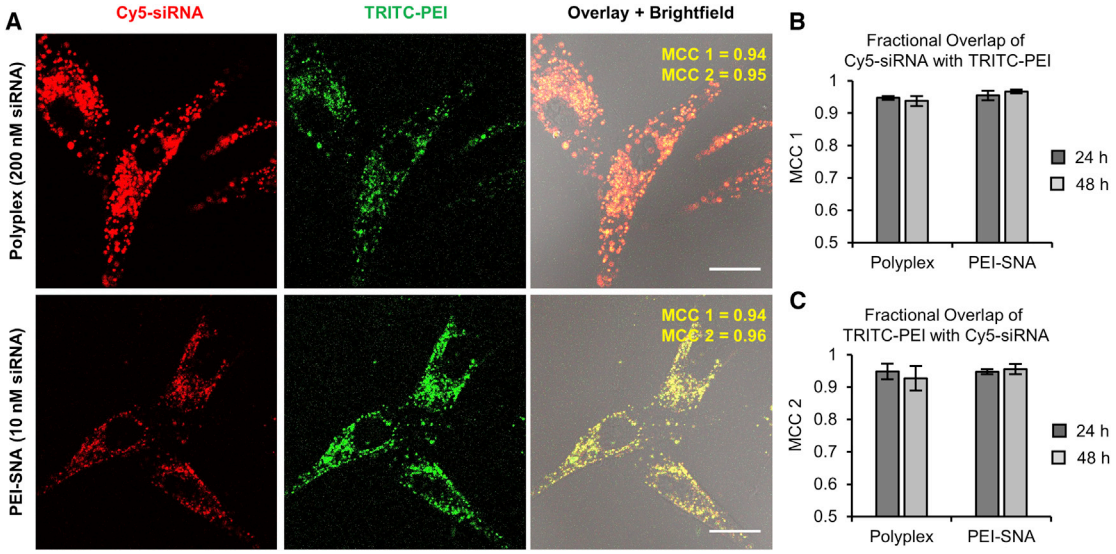

Figure 4. Relative Trafficking of siRNA and PEI from PEI-SNAs versus Polyplexes

(A) Representative confocal microscopy images showing that Cy5-siRNA remains mostly colocalized with TRITC-PEI from both polyplexes and PEI-SNAs following 24-hr incubation with cells (scale bars, 20 μm). Manders' colocalization coefficient for fractional overlap of Cy5-siRNA and TRITC-PEI is shown in yellow on the merged bright-field image (MCC 1, Cy5-siRNA colocalized with TRITC-PEI; MCC 2, TRITC-PEI colocalized with Cy5-siRNA). Quantitative assessment of colocalization depicting average fractional overlap of (B) Cy5-siRNA with TRITC-PEI (MCC 1) and (C) TRITC-PEI with Cy5-siRNA (MCC 2) in cells exposed to PEI-SNAs or polyplexes for 24 or 48 hr across three independent replicates ± SDs; no significant differences by Student's t test.

harvested and analyzed for GFP expression by flow cytometry. PEI-SNAs induced a significant decrease in GFP fluorescence at a low dose of 32 nM siRNA and yielded an impressive 70% reduction in GFP relative to untreated cells when dosed at 60 nM siRNA (Figures 6A and 6C). Interestingly, polyplex-mediated RNAi required nearly a 10-fold increase in total siRNA payload to reduce GFP expression. At siRNA doses up to 200 nM, no silencing was observed. At siRNA doses of 500 and 1,000 nM, significant GFP silencing was observed, and GFP intensity was reduced by 81% relative to untreated cells (Figures 6B and 6D). From this data, we calculated the siRNA dosage required to achieve 50% gene silencing from either carrier (ED_{50}) and found that 38 nM siRNA is required to achieve 50% GFP silencing via PEI-SNAs, while 403 nM siRNA is required via polyplexes (Figures 6B and 6D). For comparison, 400 nM siRNA delivered via SNAs lacking a PEI coating was insufficient to silence GFP expression under the conditions tested (Figure S6). Our studies demonstrate that PEI-SNAs enhance polycation-mediated GFP silencing by 10-fold. We attribute the dramatically enhanced silencing potency of PEI-SNAs relative to polyplexes to the unique three-dimensional presentation of siRNAs and polycations in this system.

PEI-SNAs Improve Polycation Cytocompatibility Relative to Polyplexes

The cytocompatibility profiles of PEI-SNAs and polyplexes were evaluated by 3-(4,5)-dimethylthiazol-2-yl)-2,5-diphenyltetrazolium bromide (MTT) assay and live cell propidium iodide (PI) staining with flow cytometry analysis. PEI-SNAs are cytocompatible as indicated by insignificant changes in metabolic activity at siRNA doses up to 60 nM (corresponding to 34 μg/mL PEI) (Figure 7A). Likewise, polyplexes are cytocompatible at siRNA doses up to 750 nM (corresponding to 8 μg/mL PEI) (Figure 7B). MTT assay results were further used to calculate half-maximal inhibitory concentration (IC_{50}) values for both PEI-SNAs and polyplexes. PEI-SNAs exhibit an IC_{50} of 80 nM siRNA, corresponding to 45 μg/mL PEI (Figure 7A). Polyplexes exhibit an IC_{50} of 920 nM siRNA, corresponding to 9.3 μg/mL PEI (Figure 7B). The observed decreases in relative metabolic activity correlate with an increase in the fraction of PI^+ cells, supporting the results obtained by MTT assay (Figures 7C and 7D). From these studies, we conclude that both PEI-SNAs and polyplexes are cytocompatible within a dosing range sufficient for gene silencing. Further, despite the known cytotoxicity of PEI at concentrations used for nucleic acid delivery, we observed that higher PEI concentrations delivered via PEI-SNAs were more cytocompatible than lower PEI concentrations delivered via polyplexes. This may be due to enhanced electrostatic interaction with the radially oriented siRNA present on PEI-SNAs, presence of the negatively charged AuNP core, or altered presentation of the PEI molecules to cells. This intriguing result warrants future investigation of the relationship between polycation presentation from nanomaterials and cytotoxicity.

DISCUSSION

Our findings demonstrate that hybrid PEI-SNA constructs with defined siRNA architecture mediate RNAi more efficiently than randomly assembled PEI-siRNA polyplexes. We observed that PEI-SNAs enable greater cellular uptake of siRNA, undergo decreased lysosomal accumulation, and efficiently silence GFP expression at

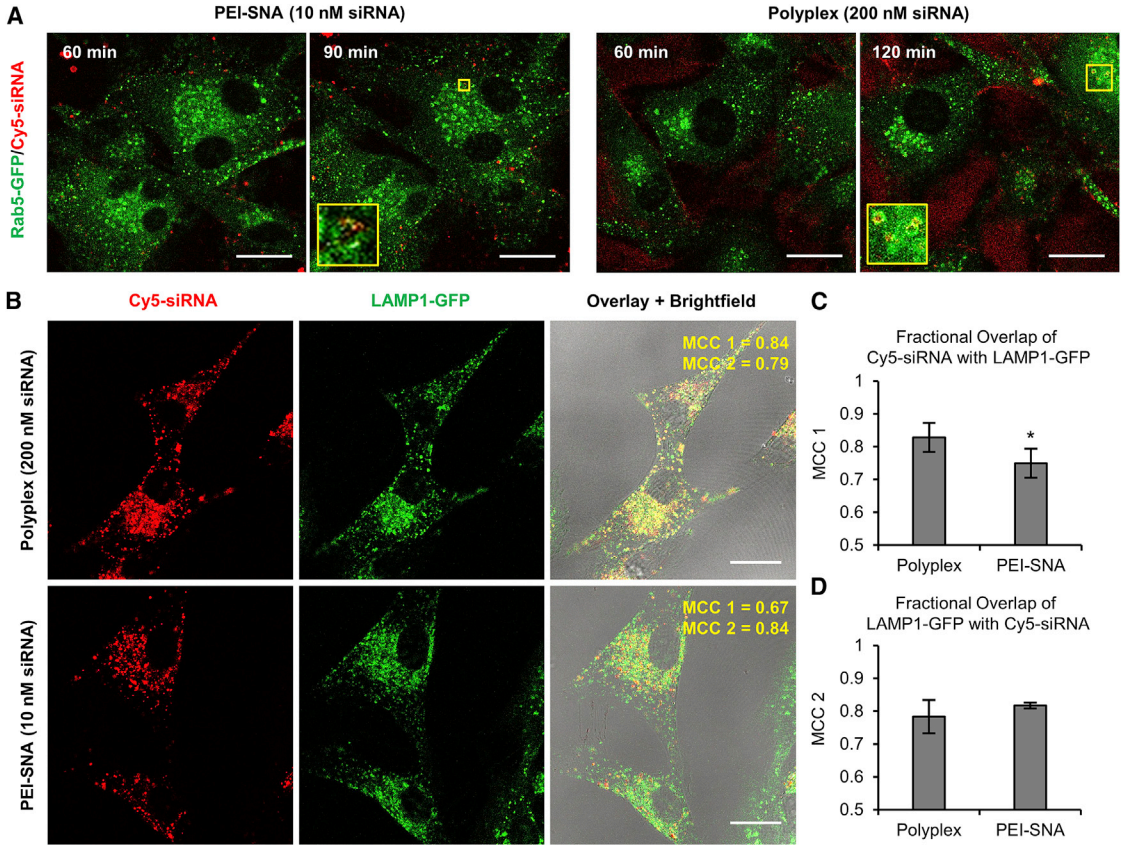

Figure 5. Intracellular Trafficking of siRNA Depends on Nanocarrier Architecture

(A) Representative confocal microscopy images showing Cy5-siRNA colocalization with early endosomes tagged via a Rab5-GFP fusion protein (scale bars, 20 μm). Yellow boxes indicate magnified regions of siRNA colocalized with Rab5$^+$ early endosomes. (B) Representative confocal microscopy images showing Cy5-siRNA colocalization with lysosomes tagged via a LAMP1-mGFP fusion protein. Areas of colocalization appear yellow in the merged bright-field image (scale bars, 20 μm). Manders' colocalization coefficient for fractional overlap of Cy5-siRNA and LAMP1-GFP is shown in yellow on the merged bright-field image (MCC 1, Cy5-siRNA colocalized with LAMP1-GFP; MCC 2, LAMP1-GFP colocalized with Cy5-siRNA). Quantitative assessment of colocalization depicting average fractional overlap of (C) Cy5-siRNA with LAMP1-GFP (MCC 1) and (D) LAMP1-GFP with Cy5-siRNA (MCC 2) across three independent replicates ± SDs; *p = 0.05 by Student's t test.

lower siRNA doses relative to polyplexes. Additionally, we found that PEI-SNAs exhibit decreased toxicity per PEI content relative to polyplexes, allowing the use of more polycation. From these results, we conclude that the architecture of siRNA nanocarriers plays an important role in their cellular interactions and ultimate gene regulation efficacy.

To understand how exposure to biological milieu will affect PEI-SNAs and polyplexes, we performed serum stability studies in which constructs were incubated in 1%, 5%, or 10% FBS for 2 hr and subsequently evaluated by zeta potential measurements and DLS. We found that serum proteins are crucial for maintaining the colloidal stability of PEI-SNAs and possibly polyplexes to a lesser extent. Following 2-hr incubation with FBS, both PEI-SNAs and polyplexes undergo charge reversal for all tested FBS concentrations (Figure 2A), indicating that negatively charged serum proteins associate with both particle types. Further, both PEI-SNAs and polyplexes exhibited significant decreases in hydrodynamic diameter after incubation with 5%–10% FBS (Figure 2B). Based on the observed charge reversal and partial hydrodynamic diameter decrease, we speculate that serum proteins displace PEI that is loosely bound to the periphery of both particle types and that this interaction induces a stabilizing effect. Because we used FBS to model exposure to physiological environments, we would expect that the observed protein corona is largely composed of BSA. While BSA is negatively charged and likely decreases the cellular adhesion of our cationic nanoparticles, it may improve their cytocompatibility by screening strong positive charges.[25] Further, incorporation of albumin around PEI-DNA and PEI-siRNA polyplexes was previously demonstrated to increase cellular uptake of polyplexes and improve transfection efficiency.[26,27] However, a limitation of our study is that FBS lacks complement proteins found in plasma, so future work should seek to understand how these proteins will interact with PEI-SNAs and polyplexes as well.

We found that cells bind and take up PEI-SNAs most rapidly and to the greatest extent of the siRNA carriers we investigated (Figure 3).

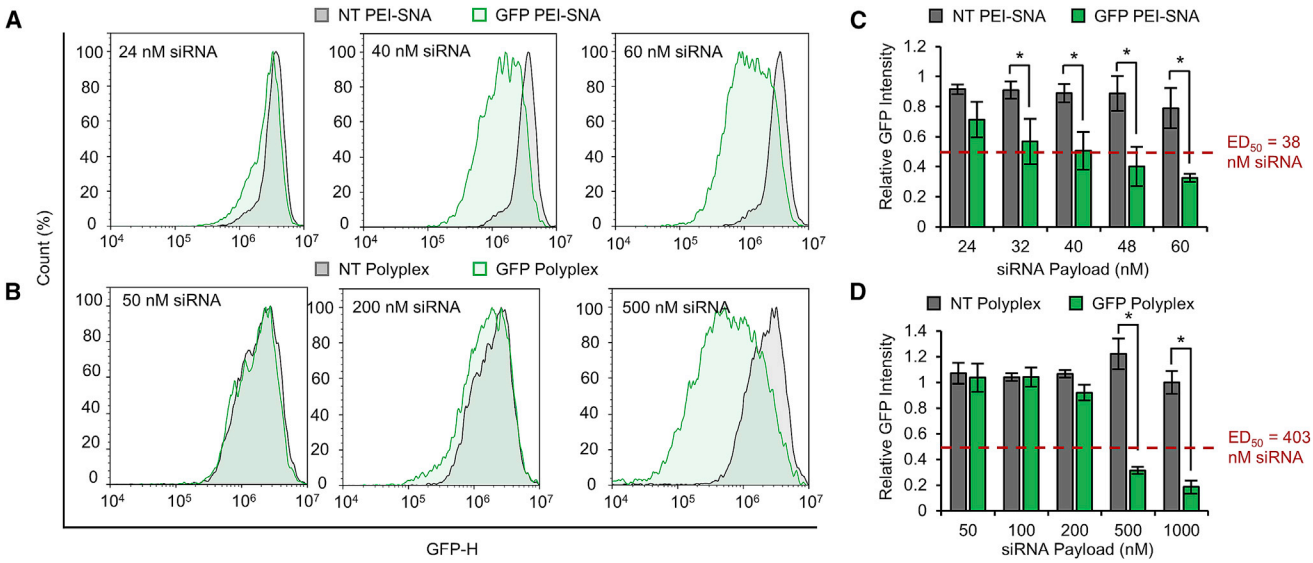

Figure 6. GFP Silencing Efficacy Assessed by Flow Cytometry Using PEI-SNAs or Polyplexes

Representative flow cytometric histograms from one representative experiment depict dose-dependent GFP silencing using (A) PEI-SNAs or (B) polyplexes. Summary flow cytometry GFP silencing results using (C) PEI-SNAs or (D) polyplexes averaged across three independent replicates ± SDs; *p < 0.01 by one-way ANOVA with post-hoc Tukey. Median fluorescence values for experimental samples are normalized to that of an untreated control.

We attribute this to several physicochemical characteristics of PEI-SNAs. Notably, cationic nanomaterials undergo greater cellular uptake than anionic nanomaterials because positively charged constructs electrostatically associate with negatively charged cell membranes to promote binding to the cell surface.[28–30] It is therefore unsurprising that cationic PEI-SNAs and polyplexes undergo enhanced cellular uptake relative to anionic SNAs (Figure 3). However, initial SNA binding and uptake was more rapid than that of polyplexes (Figure 3), demonstrating that surface charge is not the only property responsible for dictating cellular uptake. We attribute the more rapid binding and uptake of SNAs relative to polyplexes and the maximal uptake of PEI-SNAs over all carriers to the surface structure of SNAs and PEI-SNAs. SNAs contain a high density of radially oriented siRNA at their surface, and this architecture allows multiple siRNA strands from a single particle to simultaneously interact with cell surface receptors. As a result, SNAs engage in multivalent binding,[31] a property known to enhance the cellular uptake of nanomaterials.[32–34] Further, SNA architecture enhances nucleic acid secondary structure, such as G-quadruplex formation in G-rich SNAs.[35] This further engages scavenger receptors to increase cellular uptake and may explain why SNAs undergo more rapid binding and uptake than polyplexes at early time points despite their negative charge. This may also explain the enhanced binding and uptake of PEI-SNAs over polyplexes (Figure 3). Wang et al.[34] made the similar observation that ligand organization determines the uptake of peptide-targeted nanoparticles. They found that nanoparticle-bound peptide-lipids are more monomeric and deaggregated than peptide-lipids in aqueous solution, which correlated with improved cellular uptake and emphasizes the importance of ligand orientation and presentation to cells.[34] Our studies suggest that, in the siRNA carriers we investigated, both surface charge and structure play a greater role in regulating cellular interactions than nanoparticle size, another physicochemical property known to influence biological interactions of nanomaterials.[28] This is evident in that SNAs, which are optimally sized to maximize cellular uptake (50 nm; Figure 1),[36] undergo decreased binding and uptake relative to larger PEI-SNAs and polyplexes (~150 nm; Figure 1).

Finally, the differential uptake between PEI-SNAs and polyplexes could be explained by differences in the composition of each construct. The AuNP core, which serves as a template around which siRNA is spherically arranged, is present in PEI-SNAs but not in polyplexes. However, previous studies investigating the role of core materials in SNA cellular interactions suggest that the presence of the AuNP core has negligible impact on cellular binding and uptake. For example, both hollow SNAs lacking a core material and SNAs containing a quantum dot core undergo cellular uptake and intracellular trafficking similar to that of AuNP-based SNAs.[37,38] Another important composition difference between PEI-SNAs and polyplexes is the ratio of polycation to siRNA. The goal of this study was to compare optimal conditions for siRNA delivery between PEI-SNAs and polyplexes, so we synthesized polyplexes using N/P = 6/1 to achieve this goal. We chose this ratio to maximize polycation content for efficient transfection while minimizing toxicity (Figure S1) and to generate carriers of similar size and surface charge to PEI-SNAs (Figure 1B). This is in good agreement with existing literature on optimal siRNA polyplex N/P ratios.[21,39] For polyplexes generated with 25 kDa branched PEI (bPEI) and siRNA, N/P = 6/1 corresponds to 0.0101 μg/mL PEI per nM siRNA. PEI-SNAs were synthesized by incubating SNAs in excess PEI to prevent aggregation

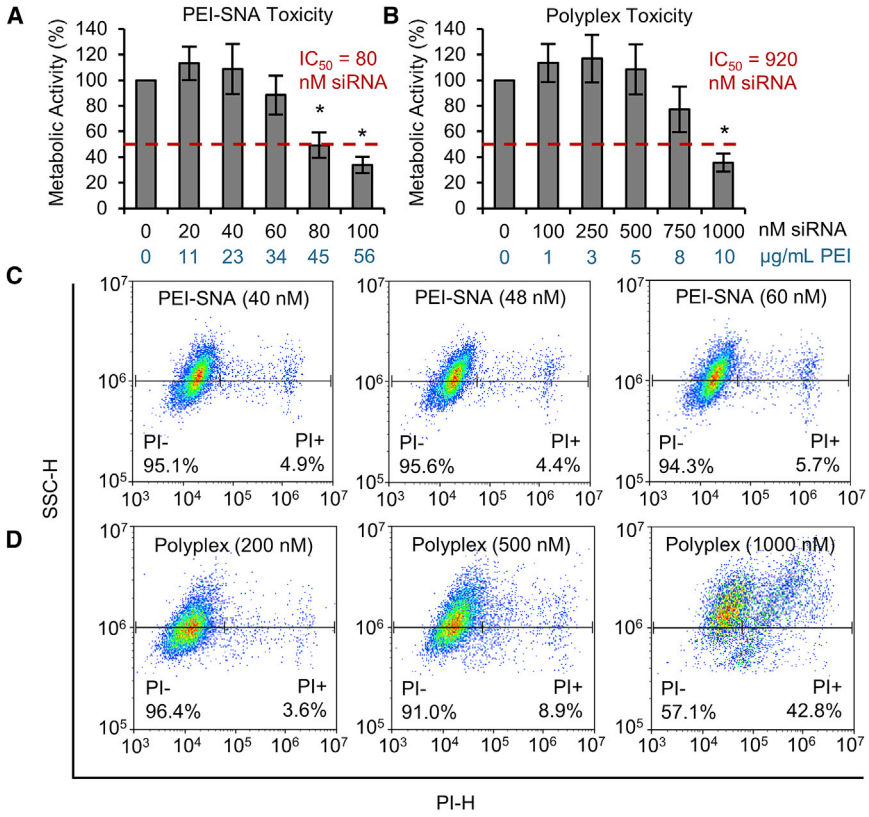

Figure 7. Cytocompatibility Profiles for PEI-SNAs and Polyplexes

The cytocompatible dosing range of both (A) PEI-SNAs and (B) polyplexes was determined using an MTT assay. Data are means ± SDs; *$p < 0.01$ by one-way ANOVA with post-hoc Tukey. Results were confirmed using PI staining and flow cytometric analysis in live cells exposed to (C) PEI-SNAs or (D) polyplexes.

due to interparticle bridging[21] then unbound PEI was removed by centrifugation to yield purified constructs. Using a TNBS assay for amine quantification, we determined that purified PEI-SNAs contain 0.55 µg/mL PEI per nM siRNA. However, despite containing higher PEI content, PEI-SNAs appear less cytotoxic than polyplexes per PEI payload. Cytocompatibility analysis found that PEI-SNAs yield an IC_{50} value of 80 nM siRNA, corresponding to 45 µg/mL PEI, while polyplexes yield an IC_{50} value of 920 nM siRNA, corresponding to 9.3 µg/mL PEI (Figures 7A and 7B). This result was surprising, given the known cytotoxicity of PEI. In agreement with our findings, alternating electrostatic assembly of siRNA and PEI or other materials designed to promote siRNA release around AuNPs has previously demonstrated reduced toxicity relative to PEI-siRNA complexes alone.[40,41] Further, previous research has demonstrated that complexing PEI with additional anionic polymers and nucleic acids also reduces PEI toxicity relative to PEI-nucleic acid complexes alone.[42,43] Based on our results and the results of others, we conclude that the presentation of PEI to cells is important in determining its cytotoxicity and that the architecture afforded by PEI-SNAs offers greater cytocompatibility than PEI assembled randomly in polyplexes.

To understand how nanocarrier architecture impacts intracellular stability, we evaluated the relative intracellular fates of siRNA and PEI from either carrier by confocal microscopy using dual-labeled PEI-SNAs and polyplexes synthesized with Cy5-siRNA and TRITC-PEI. Colocalization analysis determined that siRNA and PEI remain heavily colocalized from both carriers through 48-hr incubation with cells, as evidenced by all MCCs remaining ~0.94–0.96 (Figures 4A, 4B, and S4). This suggests that the electrostatic interactions between siRNA and PEI are strong enough to prevent significant dissociation of either carrier over the time points we investigated. While the spatial resolution of confocal microscopy may limit our ability to detect dissociation of small amounts of siRNA or PEI, our findings agree with a growing body of work that suggests strong polycation-siRNA interactions may prevent substantial intracellular dissociation. One such investigation comparing the self-assembly mechanisms of PEI-siRNA and PEI-DNA found that PEI-siRNA complexation was more thermodynamically favorable and produced more stable complexes than PEI-DNA,[39] which may explain why we do not observe significant dissociation of PEI-SNAs or polyplexes.

Moreover, the high stability of PEI-SNAs and polyplexes may be especially advantageous, given that our data shows that both complexes reside largely within lysosomes (Figure 5). An elegant Förster resonance energy transfer-based study demonstrated that PEG/PEI-DNA polyplex dissociation within the endo-lysosomal system negatively correlated with transfection efficiency.[22] This finding is corroborated by another study that found that siRNA polyplexes made with polymers containing double cationic charges per monomer bind more strongly to siRNA and improve transfection efficiency.[44] Therefore, complexes that are robust against dissociation, particularly within endo-lysosomal compartments, may prove more efficient as nucleic acid carriers.

Similarly, an unresolved challenge to siRNA delivery is reducing the net accumulation of siRNA within lysosomes, which ultimately leads to degradation of internalized siRNA. Most siRNA carriers are internalized by receptor-mediated endocytosis and are subsequently trafficked through early and late endosomes, which acidify and ultimately fuse with lysosomes. Once trapped within lysosomes, internalized cargo is degraded and rendered inactive. We found that PEI-SNAs associate with $Rab5^+$ early endosomes within

60 to 90 min, while polyplexes are first detectable in early endosomes within 120 min (Figure 5A). We further demonstrate that PEI-SNAs undergo significantly decreased lysosomal accumulation relative to polyplexes (Figures 5B–5D), suggesting that PEI-SNAs may act more efficiently as siRNA carriers. Our results are consistent with previous research investigating the use of AuNP/polycation hybrid materials for siRNA delivery. For example, one such study demonstrated that AuNPs functionalized with alternating layers of poly(allylamine hydrochloride) and siRNA or PEI and siRNA exhibited decreased colocalization with lysosomes relative to Lipofectamine 2000 or AuNPs functionalized with alternating layers of poly(diallyl dimethyl ammonium chloride) and siRNA.[45] Additionally, incorporating polymers designed to degrade at endosomal pH into AuNP-based siRNA delivery systems can further improve endosomal escape.[41,46] Because endosomal escape is well understood to be a highly inefficient process, we believe that our observed 8% decrease in PEI-SNA colocalization with lysosomes relative to polyplexes may be biologically impactful. Notably, a study investigating the intracellular trafficking of lipid nanoparticles, among the most successful and widely investigated siRNA carriers,[24] determined that only 1%–2% of internalized siRNA escapes endosomes to reach the cytosol.[23] Another study further elucidated the inefficient nature of endosomal escape through a series of experiments directly visualizing rupturing endosomes. This study determined that lipoplex-mediated siRNA delivery induces between 1 and 5 endosomal escape events per cell over a period of several hours and that endosomes that do rupture only release about half of their internalized siRNA.[47] Therefore, given the documented inefficiency of endosomal escape, we hypothesize that the observed 8% decrease in lysosomal accumulation afforded by PEI-SNAs is biologically significant and likely contributes to their enhanced gene-silencing potency.

Finally, gene-silencing studies demonstrated that PEI-SNAs enhance siRNA-mediated GFP silencing by 10-fold. Our data shows that 38 nM siRNA is required to achieve 50% GFP silencing via PEI-SNAs, while 403 nM siRNA is required via polyplexes (Figures 6B and 6D). The high siRNA dose required by polyplex-mediated gene silencing is consistent with what others have observed for PEI-based polyplexes; for example, one study reported that at least 200 nM siRNA was required to silence luciferase gene expression using 25 kDa bPEI polyplexes.[21] Interestingly, another study demonstrated that 25 kDa bPEI was insufficient to silence luciferase expression, while robust gene silencing was observed using PEI modified by succinylation at 10% of amines.[8] This improved silencing efficacy was attributed to the decrease in toxicity afforded by succinylation, enabling the use of more polycation. Our results and the results of others further support this conclusion, suggesting that improving the cytocompatibility of PEI by chemical or structural modification is a promising strategy to enhance siRNA delivery.[4] Our studies reveal that improving the cytocompatibility of PEI by altering its presentation to cells can enhance the net cellular uptake of siRNA and reduce lysosomal accumulation to dramatically enhance gene silencing potency.

While our investigation sought to evaluate the role of siRNA architecture in polycation-mediated gene silencing at the cellular level, future research should employ animal models to determine the role of nanocarrier architecture on biodistribution and gene regulation efficacy at a disease site. One recent investigation of ligand presentation for RNA targeting to tumors demonstrated the importance of RNA orientation in maximizing ligand exposure to biological systems.[48] Similarly, another study determined that AuNPs functionalized with siRNA/PEG-poly(L-lysine)-thiol complexes exhibited significantly greater intratumoral accumulation following intravenous injection than siRNA/PEG-poly(L-lysine) polyplexes.[49] Because these constructs exhibit architecture similar to PEI-SNAs, we would expect to see similar results using our system.

In conclusion, nanocarrier architecture and the resulting orientation of therapeutic cargo can be engineered to promote siRNA delivery. To demonstrate this, we compared the cellular interactions of two PEI-based siRNA carriers with similar size and surface charge but different architecture: PEI-SNAs, in which PEI is wrapped around a highly oriented SNA nanoparticle core and randomly assembled PEI-siRNA polyplexes lacking controlled architecture. We found that PEI-SNAs undergo enhanced and more rapid cellular uptake than polyplexes. Cellular uptake of nanoparticles is broadly understood to rely on size and surface charge, but our evidence suggests a prominent role for architecture as well. We further demonstrate using confocal microscopy studies that while PEI-SNAs and polyplexes exhibit similar intracellular stability as evidenced by colocalization analysis of fluorescent siRNA and PEI, PEI-SNAs undergo decreased accumulation within lysosomes, identifying another advantage conferred by their architecture. Indeed, these advantageous cellular interactions enhanced the siRNA delivery potency of PEI-SNAs by 10-fold relative to polyplexes. Finally, cytocompatibility studies suggest that the association of PEI with a complex SNA core decreases its cytotoxicity relative to PEI-based polyplexes, allowing the use of more polycation. Our studies provide critical insight into a novel design parameter for engineering siRNA carriers based on polycations and warrant future investigation of nanocarrier architecture on cellular-, organ-, and organism-level interactions.

MATERIALS AND METHODS

SNA and PEI-SNA Synthesis and Characterization

Fifteen-nanometer AuNPs were synthesized using the Frens method.[18] In brief, gold chloride (Sigma Aldrich, St. Louis, MO) was dissolved in deionized (DI) water and brought to a boil under reflux. Sodium citrate was added while stirring vigorously, and the solution reacted for 15 min until the color changed from pale yellow to deep red. AuNPs were filtered to remove large aggregates and treated with 0.1% diethyl pyrocarbonate (DEPC) (Sigma Aldrich, St. Louis, MO) overnight to inactivate RNases. SNAs were prepared by suspending 10 nM AuNPs in 0.1% Tween 20 and 150 mM NaCl. Thiolated siRNA duplexes (1–1.75 nmol/mL to normalize loading across sequences) (Integrated DNA Technologies, Coralville, IA) were added, and NaCl was increased over time to 350 mM. Finally, SNAs were passivated with 30 μM 2 kDa methoxy-polyethylene

glycol-thiol (mPEG-SH; Laysan Bio, Arab, AL) and purified by sequential centrifugation (21,000 × *g*, 30 min) and resuspension in PBS to remove unbound molecules. Following purification, PEI-SNAs were synthesized by adding 1 mg/mL 25-kDa branched PEI (Sigma Aldrich, St. Louis, MO) to 10 nM SNAs and incubating for 15 min under sonication to prevent aggregation. PEI-SNAs were subsequently purified by centrifugation to remove unbound PEI. siRNA sequences used are as follows: GFP, 5′-GGC UAC GUC CAG GAG CGC ACC-3′ dTdT; Scr, 5′-ACG CGA CCG UGC CGA UCG GCA-3′ dTdT; Negative Control siRNA #1 (Thermo Fisher Scientific, Waltham, MA).

The number of RNA duplexes per SNA was determined using a Quant-IT OliGreen assay (Thermo Fisher Scientific, Waltham, MA) as previously described.[19] In brief, SNAs were heated to 45°C in 8 M urea to dehybridize the siRNA. SNAs were pelleted by centrifugation and the antisense-containing supernatant was collected. Supernatant samples were incubated with components of the OliGreen kit and the sample fluorescence intensity was compared to that of an antisense standard curve to determine the number of intact siRNA duplexes per SNA. The amount of PEI per SNA was determined using a 2,4,6-trinitrobenzene sulfonic acid TNBS assay for colorimetric amine detection as described previously.[20] In brief, PEI-containing supernatant was collected during PEI-SNA purification and diluted in MES buffer (0.1 M MES, 0.15 M NaCl [pH 4.7]). Samples were incubated with 0.025 w/v% TNBS (30 min at 37°C [pH 9.5]), and the reaction was stopped with SDS and HCl. The sample absorbance at 344 nm was measured and compared to that of a PEI standard curve to determine the amount of PEI remaining in the supernatant following PEI-SNA collection.

PEI-siRNA Polyplex Synthesis

PEI-siRNA polyplexes were prepared using standard methods.[21] siRNA and PEI were diluted separately in 10 mM 4-(2-hydroxyethyl)-1-piperazineethanesulfonic acid) (HEPES) buffer (at pH 7.2), then combined at an N/P ratio of 6/1, vortexed for 5 s, and incubated at room temperature for 20 min. Polyplexes were further diluted in HEPES buffer for characterization or cell culture medium for experiments without further purification.

Particle Characterization and Evaluation of Serum Stability

Samples were prepared for TEM imaging by incubating a drop of sample solution on a poly-L-lysine-coated 400 mesh formvar copper grid (Electron Microscopy Sciences, Hatfield, PA). Grids were subsequently dried and counterstained with 2% uranyl acetate prior to imaging on a Zeiss LIBRA 120 TEM. AuNPs, SNAs, and PEI-SNAs were characterized by UV-visible spectroscopy using a Cary 60 spectrophotometer (Agilent Technologies, Santa Clara, CA). DLS and zeta potential measurements were made using a Litesizer500 (Anton Paar, Graz, Austria). SNAs and PEI-SNAs were diluted in DI water to 0.67 nM for DLS or to 1.6 nM for zeta potential measurements. Polyplexes were diluted in HEPES buffer to a final RNA concentration of 200 nM for DLS or to 333 nM for zeta potential measurements. Zeta potential measurements were replicated at least eight times per sample or until quality criteria was met. Serum stability was evaluated by incubating particles in 0%, 1%, 5%, or 10% FBS diluted in PBS for 2 hr at 37°C with gentle shaking. Samples were further diluted in PBS to the concentrations described above for DLS and zeta potential analysis.

Cell Culture and Stable Gene Expression

U87-MG and U373 glioma cells (ATCC, Manassas, VA) and 293TN cells (System Biosciences, Palo Alto, CA) were cultured in DMEM (VWR, Radnor, PA) supplemented with 10% FBS (Gemini Bio-Products, West Sacramento, CA) and 1% penicillin/streptomycin (Thermo Fisher Scientific, Waltham, MA). Cells were maintained in a humidified environment at 37°C, 5% CO_2. U373 cells were stably transfected with EGFP as described previously.[50–52] In brief, cells were transfected with a murine stem cell virus (MSCV) retroviral vector encoding an EGFP-Firefly luciferase fusion protein and sorted for EGFP positivity. U87-MG cells were stably transfected with Rab5-GFP or LAMP1-GFP using standard procedures. In brief, Rab5-GFP (Addgene # 56530) or LAMP1-GFP (Addgene # 34831) was cloned into a lentiviral transfer vector (System Biosciences, Palo Alto, CA) by restriction enzyme digest. Lentiviral particles were produced by triple-transfecting (TransIT-Lenti transfection reagent; Mirus Bio, Madison, WI) 293TN cells with either transfer vector and lentiviral packaging and envelope plasmids (Addgene #12260,12259). Lentivirus was harvested, filtered, and diluted in cell culture medium to transduce U87-MG cells. Cells stably expressing the desired fusion protein were selected with 1 μg/mL puromycin (VWR, Radnor, PA).

Cellular Uptake Analysis

U87-MG cells were seeded in 24-well culture plates at a density of 50,000 cells/well and cultured overnight. Cells were incubated with SNAs, PEI-SNAs, or PEI-siRNA polyplexes labeled with Cy5-siRNA (Integrated DNA Technologies, Coralville, IA) diluted in complete culture medium at concentrations normalized to siRNA payload (20 nM siRNA) for various times ranging from 15 min to 24 hr at 37°C, 5% CO_2. Cells were washed with PBS, trypsinized, and resuspended in PBS for Cy5 intensity analysis by flow cytometry using a NovoCyte flow cytometer (ACEA Biosciences, San Diego, CA).

Lysosomal Trafficking and Imaging

U87 cells expressing Rab5-GFP or LAMP1-GFP were seeded in 35 mm glass bottom dishes at a density of 150,000 cells/dish and cultured overnight in a humidified incubator. Cells were incubated with PEI-SNAs (10 nM siRNA) or polyplexes (200 nM siRNA) prepared with Cy5-siRNA for 0 to 24 hr at 37°C, 5% CO_2, washed three times with PBS to remove uninternalized constructs, counterstained with CellMask Orange (Thermo Fisher Scientific, Waltham, MA), and fed with phenol-red-free complete medium. Live cell imaging was performed using a Zeiss LSM880 confocal microscope equipped with an incubated stage to maintain cells during imaging. Z stacks were acquired to analyze PEI-SNA/polyplex colocalization throughout the entire volume of the cell. Quantitative colocalization analysis was used to determine the fraction of siRNA conjugates present within lysosomes and the fraction of lysosomes containing

siRNA conjugates. Image analysis was performed using three independent datasets, each consisting of 5–7 images (corresponding to 10–20 cells) per treatment group. Regions of interest (ROIs) were defined by manually tracing the outlines of individual cells (and excluding nuclei) using ImageJ[53] (NIH, Bethesda, MD) and imported into MATLAB (MathWorks, Natick, MA) for quantitative colocalization analysis using a custom script. Both the Cy5-PEI-SNA/polyplex and LAMP1-GFP channels were median filtered with a 3-by-3-by-3 neighborhood and top-hat filtered by reconstruction using a 2-μm disk element. Manders' colocalization coefficients[54] were calculated for each ROI within each image stack, and all ROIs for each treatment group were averaged within an experimental replicate. Statistics were performed across averages from three independent replicates.

siRNA and PEI Cotrafficking Analysis

Intracellular construct stability was evaluating by observing the relative intracellular fates of siRNA and PEI by confocal microscopy. PEI was labeled with TRITC using previously reported methods.[55] In brief, PEI (1 mL at 10 mg/mL in DI water) was reacted with TRITC (11 μL at 10 mg/mL in DMF) overnight to label 1% of the primary amines. The product was lyophilized and stored dried at −20°C until resuspension in DI water for experiments. PEI-SNAs and polyplexes were synthesized using TRITC-PEI and Cy5-siRNA as previously described. For siRNA and PEI co-trafficking analysis, U87-MG cells were seeded in 35-mm glass bottom dishes at a density of 150,000 cells/dish and cultured overnight. Cells were incubated with PEI-SNAs (10 nM siRNA) or polyplexes (200 nM siRNA) prepared with Cy5-siRNA for 24 hr at 37°C, 5% CO_2, washed three times with PBS to remove uninternalized constructs, and fed with fresh medium. Cells were either imaged immediately or incubated for an additional 24 hr prior to imaging. Confocal microscopy was performed and quantitative colocalization analysis was conducted as described above.

Toxicity Assessment

U87-MG cells were seeded in 96-well culture plates at a density of 2,500 cells/well and cultured overnight. Cells were incubated with PEI-SNAs or PEI-siRNA polyplexes in complete culture medium for 24 hr at 37°C, 5% CO_2. Construct-containing medium was removed, and cells were replenished with fresh medium then incubated a further 24 hr at 37°C, 5% CO_2. Cellular metabolic activity was assessed by MTT assay (Thermo Fisher Scientific, Waltham, MA) according to the manufacturer's protocol. These results were corroborated by live cell PI staining to detect cells that have undergone membrane permeabilization. U373.eGFP cells were exposed to PEI-SNAs or polyplexes under the previously stated conditions, then trypsinized, stained with PI, and analyzed by flow cytometry using a NovoCyte flow cytometer. IC_{50} values for PEI-SNAs and polyplexes were calculated using MATLAB software.

Gene Knockdown Assessment

U373.eGFP cells were seeded in 12-well culture plates at a density of 25,000 cells/well and cultured overnight. Cells were incubated with PEI-SNAs or PEI-siRNA polyplexes diluted in complete culture medium for 24 hr at 37°C, 5% CO_2. PEI-SNA- or polyplex-containing medium was removed, and cells were replenished with fresh complete culture medium and incubated a further 24 hr at 37°C, 5% CO_2. Cells were trypsinized and resuspended in PBS for GFP intensity analysis by flow cytometry using a NovoCyte flow cytometer.

Statistical Analysis

All experiments were repeated in triplicate and data are reported as means ± SD across three independent replicates unless otherwise stated. Groups with significant differences were determined using Student's t test (when two groups were compared) and one-way ANOVA with post-hoc Tukey test (when three or more groups were compared) completed in MATLAB software (MathWorks, Natick, MA). Differences were considered significant at $p < 0.05$. Flow cytometry data was analyzed using NovoExpress software (ACEA Biosciences, San Diego, CA). DLS and zeta potential data were analyzed using Kalliope software (Anton Paar, Graz, Austria).

SUPPLEMENTAL INFORMATION

Supplemental Information includes Supplemental Materials and Methods and six figures and can be found with this article online at https://doi.org/10.1016/j.omtn.2018.05.008.

AUTHOR CONTRIBUTIONS

Conceptualization, J.R.M., E.S.D.; Methodology, J.R.M., N.L.K., R.G.; Investigation, J.R.M., N.L.K., R.G.; Writing – Original Draft, J.R.M., N.L.K.; Writing – Review & Editing, J.R.M., N.L.K., R.G., E.S.D.; Funding Acquisition, E.S.D.; Resources, E.S.D.; Supervision, J.R.M., E.S.D.

CONFLICTS OF INTEREST

The authors have no conflict of interest.

ACKNOWLEDGMENTS

This project was supported by the National Institutes of General Medical Sciences of the NIH under an Institutional Development Award (IDeA) (grant number U54-GM104941) and a Maximizing Investigators' Research Award (MIRA) (grant number R35-GM119659). Microscopy access was supported by grants from the NIH-NIGMS (P20 GM103446), including a shared instrumentation grant (S10 OD016361), the NSF (IIA-1301765), and the State of Delaware. We thank Shannon Modla in the Bio-Imaging Center for assistance with TEM. J.R.M. received support from the Department of Defense through a National Defense Science and Engineering Graduate Fellowship. N.L.K. received support from the University of Delaware Summer Scholars program and a National Science Foundation REU through NSF REU site: DARE TO BE FIRST 1460757. The content is solely the responsibility of the authors and does not necessarily represent the views of the funding agencies.

REFERENCES

1. Whitehead, K.A., Langer, R., and Anderson, D.G. (2009). Knocking down barriers: advances in siRNA delivery. Nat. Rev. Drug Discov. *8*, 129–138.

2. Yin, H., Kanasty, R.L., Eltoukhy, A.A., Vegas, A.J., Dorkin, J.R., and Anderson, D.G. (2014). Non-viral vectors for gene-based therapy. Nat. Rev. Genet. *15*, 541–555.
3. Wittrup, A., and Lieberman, J. (2015). Knocking down disease: a progress report on siRNA therapeutics. Nat. Rev. Genet. *16*, 543–552.
4. Hall, A., Lächelt, U., Bartek, J., Wagner, E., and Moghimi, S.M. (2017). Polyplex evolution: understanding biology, optimizing performance. Mol. Ther. *25*, 1476–1490.
5. Neuberg, P., and Kichler, A. (2014). Recent developments in nucleic acid delivery with polyethylenimines. In Advances in Genetics, Volume 88, L. Huang, D. Liu, and E. Wagner, eds. (Elsevier), pp. 263–288.
6. Singh, B., Maharjan, S., Park, T.E., Jiang, T., Kang, S.K., Choi, Y.J., and Cho, C.S. (2015). Tuning the buffering capacity of polyethylenimine with glycerol molecules for efficient gene delivery: staying in or out of the endosomes. Macromol. Biosci. *15*, 622–635.
7. Benjaminsen, R.V., Mattebjerg, M.A., Henriksen, J.R., Moghimi, S.M., and Andresen, T.L. (2013). The possible "proton sponge " effect of polyethylenimine (PEI) does not include change in lysosomal pH. Mol. Ther. *21*, 149–157.
8. Zintchenko, A., Philipp, A., Dehshahri, A., and Wagner, E. (2008). Simple modifications of branched PEI lead to highly efficient siRNA carriers with low toxicity. Bioconjug. Chem. *19*, 1448–1455.
9. Giljohann, D.A., Seferos, D.S., Prigodich, A.E., Patel, P.C., and Mirkin, C.A. (2009). Gene regulation with polyvalent siRNA-nanoparticle conjugates. J. Am. Chem. Soc. *131*, 2072–2073.
10. Cutler, J.I., Zhang, K., Zheng, D., Auyeung, E., Prigodich, A.E., and Mirkin, C.A. (2011). Polyvalent nucleic acid nanostructures. J. Am. Chem. Soc. *133*, 9254–9257.
11. Seferos, D.S., Prigodich, A.E., Giljohann, D.A., Patel, P.C., and Mirkin, C.A. (2009). Polyvalent DNA nanoparticle conjugates stabilize nucleic acids. Nano Lett. *9*, 308–311.
12. Barnaby, S.N., Lee, A., and Mirkin, C.A. (2014). Probing the inherent stability of siRNA immobilized on nanoparticle constructs. Proc. Natl. Acad. Sci. USA *111*, 9739–9744.
13. Barnaby, S.N., Perelman, G.A., Kohlstedt, K.L., Chinen, A.B., Schatz, G.C., and Mirkin, C.A. (2016). Design considerations for RNA spherical nucleic acids (SNAs). Bioconjug. Chem. *27*, 2124–2131.
14. Lee, J.S., Green, J.J., Love, K.T., Sunshine, J., Langer, R., and Anderson, D.G. (2009). Gold, poly(beta-amino ester) nanoparticles for small interfering RNA delivery. Nano Lett. *9*, 2402–2406.
15. Jensen, S.A., Day, E.S., Ko, C.H., Hurley, L.A., Luciano, J.P., Kouri, F.M., Merkel, T.J., Luthi, A.J., Patel, P.C., Cutler, J.I., et al. (2013). Spherical nucleic acid nanoparticle conjugates as an RNAi-based therapy for glioblastoma. Sci. Transl. Med. *5*, 209ra152.
16. Kouri, F.M., Hurley, L.A., Daniel, W.L., Day, E.S., Hua, Y., Hao, L., Peng, C.Y., Merkel, T.J., Queisser, M.A., Ritner, C., et al. (2015). miR-182 integrates apoptosis, growth, and differentiation programs in glioblastoma. Genes Dev. *29*, 732–745.
17. Northwestern University (2017). NU-0129 in treating patients with recurrent glioblastoma or gliosarcoma undergoing surgery. National Library of Medicine, https://clinicaltrials.gov/ct2/show/NCT0302001717.
18. Frens, G. (1973). Controlled nucleation for the regulation of the particle size in monodisperse gold suspensions. Nat. Phys. Sci (Lond.) *241*, 20–22.
19. Melamed, J.R., Riley, R.S., Valcourt, D.M., Billingsley, M.M., Kreuzberger, N.L., and Day, E.S. (2017). Quantification of siRNA duplexes bound to gold nanoparticle surfaces. Methods Mol. Biol. *1570*, 1–15.
20. Grotzky, A., Manaka, Y., Fornera, S., Willeke, M., and Walde, P. (2010). Quantification of α-polylysine: a comparison of four UV/Vis spectrophotometric methods. Anal. Methods *2*, 1448–1455.
21. Grayson, A.C., Doody, A.M., and Putnam, D. (2006). Biophysical and structural characterization of polyethylenimine-mediated siRNA delivery in vitro. Pharm. Res. *23*, 1868–1876.
22. Ulasov, A.V., Khramtsov, Y.V., Trusov, G.A., Rosenkranz, A.A., Sverdlov, E.D., and Sobolev, A.S. (2011). Properties of PEI-based polyplex nanoparticles that correlate with their transfection efficacy. Mol. Ther. *19*, 103–112.
23. Gilleron, J., Querbes, W., Zeigerer, A., Borodovsky, A., Marsico, G., Schubert, U., Manygoats, K., Seifert, S., Andree, C., Stöter, M., et al. (2013). Image-based analysis of lipid nanoparticle-mediated siRNA delivery, intracellular trafficking and endosomal escape. Nat. Biotechnol. *31*, 638–646.
24. Shi, J., Kantoff, P.W., Wooster, R., and Farokhzad, O.C. (2017). Cancer nanomedicine: progress, challenges and opportunities. Nat. Rev. Cancer *17*, 20–37.
25. Corbo, C., Molinaro, R., Parodi, A., Toledano Furman, N.E., Salvatore, F., and Tasciotti, E. (2016). The impact of nanoparticle protein corona on cytotoxicity, immunotoxicity and target drug delivery. Nanomedicine (Lond.) *11*, 81–100.
26. Syga, M.I., Nicoli, E., Kohler, E., and Shastri, V.P. (2016). Albumin incorporation in polyethylenimine-DNA polyplexes influences transfection efficiency. Biomacromolecules *17*, 200–207.
27. Polyplexes, P., Nicoli, E., Syga, M.I., Bosetti, M., and Shastri, V.P. (2015). Enhanced gene silencing through human serum albumin-mediated delivery of polyethylenimine-siRNA polyplexes. PLoS One *10*, e0122581.
28. Albanese, A., Tang, P.S., and Chan, W.C.W. (2012). The effect of nanoparticle size, shape, and surface chemistry on biological systems. Annu. Rev. Biomed. Eng. *14*, 1–16.
29. Arvizo, R.R., Miranda, O.R., Thompson, M.A., Pabelick, C.M., Bhattacharya, R., Robertson, J.D., Rotello, V.M., Prakash, Y.S., and Mukherjee, P. (2010). Effect of nanoparticle surface charge at the plasma membrane and beyond. Nano Lett. *10*, 2543–2548.
30. Gratton, S.E.A., Ropp, P.A., Pohlhaus, P.D., Luft, J.C., Madden, V.J., Napier, M.E., and DeSimone, J.M. (2008). The effect of particle design on cellular internalization pathways. Proc. Natl. Acad. Sci. USA *105*, 11613–11618.
31. Patel, P.C., Giljohann, D.A., Daniel, W.L., Zheng, D., Prigodich, A.E., and Mirkin, C.A. (2010). Scavenger receptors mediate cellular uptake of polyvalent oligonucleotide-functionalized gold nanoparticles. Bioconjug. Chem. *21*, 2250–2256.
32. Chakrabarti, A., Witsenburg, J.J., Sinzinger, M.D., Richter, M., Wallbrecher, R., Cluitmans, J.C., Verdurmen, W.P.R., Tanis, S., Adjobo-Hermans, M.J.W., Rademann, J., and Brock, R. (2014). Multivalent presentation of the cell-penetrating peptide nona-arginine on a linear scaffold strongly increases its membrane-perturbing capacity. Biochim. Biophys. Acta *1838*, 3097–3106.
33. Giljohann, D.A., Seferos, D.S., Patel, P.C., Millstone, J.E., Rosi, N.L., and Mirkin, C.A. (2007). Oligonucleotide loading determines cellular uptake of DNA-modified gold nanoparticles. Nano Lett. *7*, 3818–3821.
34. Wang, M., Miller, A.D., and Thanou, M. (2013). Effect of surface charge and ligand organization on the specific cell-uptake of uPAR-targeted nanoparticles. J. Drug Target. *21*, 684–692.
35. Chinen, A.B., Guan, C.M., and Mirkin, C.A. (2015). Spherical nucleic acid nanoparticle conjugates enhance G-quadruplex formation and increase serum protein interactions. Angew. Chem. Int. Ed. Engl. *54*, 527–531.
36. Chithrani, B.D., and Chan, W.C.W. (2007). Elucidating the mechanism of cellular uptake and removal of protein-coated gold nanoparticles of different sizes and shapes. Nano Lett. *7*, 1542–1550.
37. Young, K.L., Scott, A.W., Hao, L., Mirkin, S.E., Liu, G., and Mirkin, C.A. (2012). Hollow spherical nucleic acids for intracellular gene regulation based upon biocompatible silica shells. Nano Lett. *12*, 3867–3871.
38. Wu, X.A., Choi, C.H.J., Zhang, C., Hao, L., and Mirkin, C.A. (2014). Intracellular fate of spherical nucleic acid nanoparticle conjugates. J. Am. Chem. Soc. *136*, 7726–7733.
39. Zheng, M., Pavan, G.M., Neeb, M., Schaper, A.K., Danani, A., Klebe, G., Merkel, O.M., and Kissel, T. (2012). Targeting the blind spot of polycationic nanocarrier-based siRNA delivery. ACS Nano *6*, 9447–9454.
40. Elbakry, A., Zaky, A., Liebl, R., Rachel, R., Goepferich, A., and Breunig, M. (2009). Layer-by-layer assembled gold nanoparticles for siRNA delivery. Nano Lett. *9*, 2059–2064.
41. Chen, Z., Zhang, L., He, Y., Shen, Y., and Li, Y. (2015). Enhanced shRNA delivery and ABCG2 silencing by charge-reversible layered nanocarriers. Small *11*, 952–962.
42. Patnaik, S., Arif, M., Pathak, A., Kurupati, R., Singh, Y., and Gupta, K.C. (2010). Cross-linked polyethylenimine-hexametaphosphate nanoparticles to deliver nucleic acids therapeutics. Nanomedicine (Lond.) *6*, 344–354.
43. Tripathi, S.K., Goyal, R., Ansari, K.M., Ravi Ram, K., Shukla, Y., Chowdhuri, D.K., and Gupta, K.C. (2011). Polyglutamic acid-based nanocomposites as efficient non-viral gene carriers in vitro and in vivo. Eur. J. Pharm. Biopharm. *79*, 473–484.

44. Varkouhi, A.K., Mountrichas, G., Schiffelers, R.M., Lammers, T., Storm, G., Pispas, S., and Hennink, W.E. (2012). Polyplexes based on cationic polymers with strong nucleic acid binding properties. Eur. J. Pharm. Sci. *45*, 459–466.

45. Zhao, E., Zhao, Z., Wang, J., Yang, C., Chen, C., Gao, L., Feng, Q., Hou, W., Gao, M., and Zhang, Q. (2012). Surface engineering of gold nanoparticles for in vitro siRNA delivery. Nanoscale *4*, 5102–5109.

46. Han, L., Zhao, J., Zhang, X., Cao, W., Hu, X., Zou, G., Duan, X., and Liang, X.J. (2012). Enhanced siRNA delivery and silencing gold-chitosan nanosystem with surface charge-reversal polymer assembly and good biocompatibility. ACS Nano *6*, 7340–7351.

47. Wittrup, A., Ai, A., Liu, X., Hamar, P., Trifonova, R., Charisse, K., Manoharan, M., Kirchhausen, T., and Lieberman, J. (2015). Visualizing lipid-formulated siRNA release from endosomes and target gene knockdown. Nat. Biotechnol. *33*, 870–876.

48. Pi, F., Binzel, D.W., Lee, T.J., Li, Z., Sun, M., Rychahou, P., Li, H., Haque, F., Wang, S., Croce, C.M., et al. (2018). Nanoparticle orientation to control RNA loading and ligand display on extracellular vesicles for cancer regression. Nat. Nanotechnol. *13*, 82–89.

49. Kim, H.J., Takemoto, H., Yi, Y., Zheng, M., Maeda, Y., Chaya, H., Hayashi, K., Mi, P., Pittella, F., Christie, R.J., et al. (2014). Precise engineering of siRNA delivery vehicles to tumors using polyion complexes and gold nanoparticles. ACS Nano *8*, 8979–8991.

50. Day, E.S., Zhang, L., Thompson, P.A., Zawaski, J.A., Kaffes, C.C., Gaber, M.W., Blaney, S.M., West, J.L., et al. (2012). Vascular-targeted photothermal therapy of an orthotopic murine glioma model. Nanomedicine (Lond.) *7*, 1133–1148.

51. Day, E.S., Thompson, P.A., Zhang, L., Lewinski, N.A., Ahmed, N., Drezek, R.A., Blaney, S.M., and West, J.L. (2011). Nanoshell-mediated photothermal therapy improves survival in a murine glioma model. J. Neurooncol. *104*, 55–63.

52. Ahmed, N., Ratnayake, M., Savoldo, B., Perlaky, L., Dotti, G., Wels, W.S., Bhattacharjee, M.B., Gilbertson, R.J., Shine, H.D., Weiss, H.L., et al. (2007). Regression of experimental medulloblastoma following transfer of HER2-specific T cells. Cancer Res. *67*, 5957–5964.

53. Schindelin, J., Arganda-Carreras, I., Frise, E., Kaynig, V., Longair, M., Pietzsch, T., Preibisch, S., Rueden, C., Saalfeld, S., Schmid, B., et al. (2012). Fiji: an open-source platform for biological-image analysis. Nat. Methods *9*, 676–682.

54. Manders, E.M.M., Verbeek, F.J., and Aten, J.A. (1993). Measurement of co-localization of objects in dual-colour confocal images. J. Microsc. *169*, 375–382.

55. Goyal, R., Tripathi, S.K., Vazquez, E., Kumar, P., and Gupta, K.C. (2012). Biodegradable poly(vinyl alcohol)-polyethylenimine nanocomposites for enhanced gene expression in vitro and in vivo. Biomacromolecules *13*, 73–83.